

# Magnetization of $\text{Bi}_2\text{Sr}_2\text{CaCu}_2\text{O}_{8+\delta}$ micrometer thin ring and its depinning line

B. Semenenko <sup>\*1,2</sup>, B. C. Camargo <sup>1,3</sup>, A. Setzer <sup>1</sup>, W. Böhlmann <sup>1</sup>, Y. Kopelevich <sup>4</sup>, and P. D. Esquinazi <sup>†1</sup>

<sup>1</sup>*Felix Bloch Institute for Solid State Physics, Faculty of Physics and Earth Sciences, University of Leipzig, Linnéstraße 5, 04103, Leipzig, Germany*

<sup>2</sup>Present address: *Center of Pharmaceutical Engineering (PVZ), TU Braunschweig, Franz-Liszt-Str. 35a, 38106 Braunschweig, Germany*

<sup>3</sup>Present address: *Institute of Physics, Polish Academy of Sciences, Aleja Lotnikow 32/46, PL-02-668 Warsaw, Poland*

<sup>4</sup>*Instituto de Física “Gleb Wataghin,” Universidade Estadual de Campinas, Unicamp 13083-970, Campinas, São Paulo, Brasil*

Received: 8 April 2020 / Accepted: 23 May 2020

## Abstract

We demonstrate a geometrical effect on the depinning line (DL) of the flux line lattice of the  $\text{Bi}_2\text{Sr}_2\text{CaCu}_2\text{O}_{8+\delta}$  high- $T_c$  superconductor (HTSC) micrometer ring. The DL shifts to notably lower temperatures in comparison to bulk crystals and thin flakes of the same sample. The shift is attributed to a decrease in the overall pinning potential due to a double size effect, namely: a) the ring thickness  $\sim 1 \mu\text{m}$  being smaller than the pinning correlation length, and b) the increase in the effective London penetration depth of the vortices (Pearl vortices). The large shift of the DL to lower temperatures may influence the suitability of this HTSC for applications in microstrip antennas and THz emitters.

**Keywords**— BSCCO Depinning line Microstrip antenna Vortex dynamics THz emitter

\*semenenko@studserv.uni-leipzig.de

†esquin@physik.uni-leipzig.de

## 1 Introduction

$\text{Bi}_2\text{Sr}_2\text{CaCu}_2\text{O}_{8+\delta}$  (Bi-2212) is a high- $T_c$  superconductor (HTSC), whose magnetic and superconducting properties are still being investigated [1–9]. In particular, Bi-2212 single crystals are considered to be a key element for THz emitters devices in modern electronics [9–12]. Recently, numerical simulations and analytical calculations classified Bi-2212 micrometer rings as a class of low-loss subwavelength resonators for microstrip antennas and THz devices [2]. Although these applications are intended at zero or low applied magnetic fields, the pinning of trapped vortices within the HTSC ring should be taken into account to minimize possible losses when electromagnetic waves of large amplitude are applied.

Over the past few decades, the magnetization behaviour of superconducting rings and cylinders has been investigated theoretically [13–17] and experimentally [18–23] both in millimeter-size HTSC rings and low- $T_c$  superconducting micrometer-size rings [24]. Previous studies, done on thick Bi-2212 sam-

ples, report the presence of two thermally activated diffusion modes of the flux line lattice (FLL) that determine its depinning line (DL) [25]. In addition, an anomalous mode, associated with a phase transition at low temperatures, was observed [26]. Because different sample parameters, such as the geometry and/or defect (or doping) density [27–32], influence the response of the FLL of HTSC’s to external perturbations, its general description is complex.

In this work, we found a significant shift of the DL of the FLL of a micrometer-size and thin Bi-2212 ring to lower temperatures, which emphasizes the influence of the sample size (and eventually its geometry) on the magnetic response of this HTSC. Due to the small ring mass and consequently a low magnetic moment amplitude, we used a torque magnetometer to determine the DL at different applied fields and temperatures.

## 2 Experimental details

### 2.1 Sample processing and structural characterization

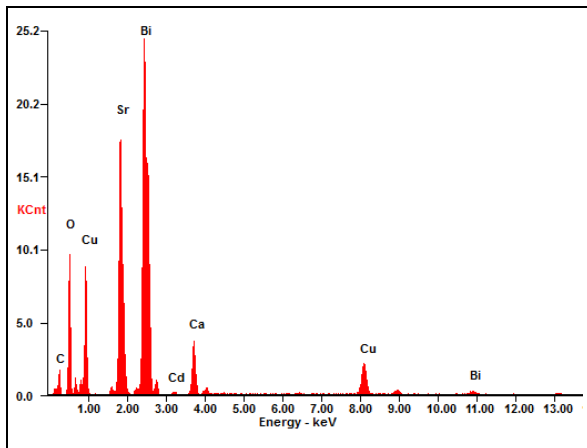


Figure 1: EDX measurements of the  $\text{Bi}_2\text{Sr}_2\text{CaCu}_2\text{O}_{8+\delta}$  crystal.

We performed energy dispersive X-ray spectroscopy (EDX) measurements to determine the composition of a bulk 2212 sample, from which flakes were

later extracted and processed in the shape of mesoscopic ring. Measurements (Figure 1) were performed with an EDX detector in the Dual Beam Microscope (DBM, Nova NanoLab 200, FEI Company), using an acceleration voltage of 15 kV. The averaged values over the sample surface show a ratio of Bi/Sr/Ca/Cu elements 2/1.7/0.8/2.2 with an error of  $\pm 0.2$ . The values agree with published characterizations on similar crystals [33, 34]. Note that the carbon peak seen in the spectrum derives from tape on which the crystal was glued and it is not an impurity of the sample.

The  $c$ -axis of each of the measured samples is oriented in the direction normal to their main area, i.e. in the direction of their thickness. The thickness, volume and mass of all measured samples are presented in Table 1. The mass of the Bi-2212 large bulk crystal was measured using a Mettler Toledo AG245 balance, whereas the masses of other samples were calculated based on the mass density  $6.71 \text{ g/cm}^3$  [35].

Table 1: The thickness, volume ( $V$ ) and mass of the samples used for magnetization measurements.

sample	thickness [ $\mu\text{m}$ ]	$V$ [ $\mu\text{m}^3$ ]	mass [g]
bulk	320	$6.5 \cdot 10^8$	$4.36 \cdot 10^{-3}$
S7	7.44	$9.0 \cdot 10^5$	$6.1 \cdot 10^{-6}$
disk	6.7	$1.3 \cdot 10^4$	$8.8 \cdot 10^{-8}$
S1	2.56	$5.6 \cdot 10^3$	$3.7 \cdot 10^{-8}$
ring	1.3	$5.6 \cdot 10^2$	$3.7 \cdot 10^{-9}$

For the preparation of the Bi-2212 ring, shown in Figure 2, we deposited a Bi-2212 flake of  $1.3 \mu\text{m}$  thickness on a Si/SiN substrate and covered it with a PMMA layer of  $1 \mu\text{m}$  thickness. The protective PMMA layer on top of the Bi-2212 flake assures that the ion beam etching procedure does not influence the material of the ring [22]. The flake with the PMMA layer was treated in air at  $120^\circ\text{C}$  for the duration of 30 min. Such treatment had a small influence on the sample critical temperature ( $T_c$ ), as evidenced by electrical resistance measurements, shown in the inset of Figure 3(a), as well as by magnetization measurement (Figure 10). The Bi-2212 ring was then prepared using a focused ion beam (FIB) with  $\text{Ga}^+$  ions accelerated with 30 kV and with a current of 0.3 nA.

The processing yielded a ring with a thickness  $t \simeq 1.3 \mu\text{m}$ , an outer diameter of  $38 \mu\text{m}$  and an inner diameter of  $30 \mu\text{m}$ . The width of the ring of  $w \simeq 4 \mu\text{m}$  was measured with by the DBM. The Bi-2212 disk was prepared by the same method as the ring with an outer diameter of  $50 \mu\text{m}$  and a thickness  $t \simeq 6.7 \mu\text{m}$ .

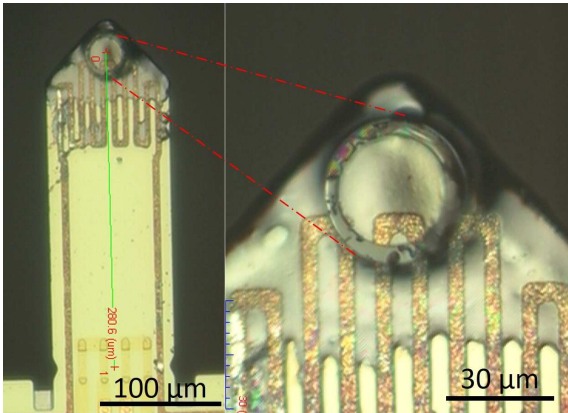


Figure 2: Optical images of the Bi-2212 micrometer ring fixed with a cryogenic vacuum grease at the edge of the cantilever of the torque magnetometer.

## 2.2 Torque magnetometer

Because Bi-2212 HTSC has a strong magnetic anisotropy (i.e., the magnetic response along the  $c$ -axis  $|m_{\parallel}|$  is much larger than the one in-plane  $|m_{\perp}|$  [36–41]), its magnetization along the sample  $c$ -axis can be investigated with torque magnetometry. To measure the magnetization, we constructed a torque magnetometer with cantilevers from the company SCL-Sensor Tech. Fabrication GmbH. Four piezoresistors on the cantilevers are part of a Wheatstone bridge, with 2 piezoresistors placed at the edge (which measures the cantilever deflection) and 2 piezoresistors on the base of the cantilever (for current compensation) [42]. Such configuration compensates the magnetic field influence on the piezoresistors, increasing the sensitivity of the system to magnetic moments of the order of  $m \sim 5 \cdot 10^{-10}$  emu at 0.1 T applied field [43]. The cantilever was fixed

in a holder inside a continuous He-flow cryostat equipped with a superconducting solenoid powered by a IPS120-10 (Oxford) power supply. For the experiments, a resistance bridge Lake Shore 370 AC, temperature controller LakeShore 340 and Keithley 2000 multimeter were used. The angle between the magnetic field and the sample was controlled by a Hall sensor installed at the sample holder.

For the torque measurements, each sample was fixed at the edge of the cantilever with vacuum grease Apiezon “H”, exemplary depicted in Figure 2. All measurements with the torque magnetometer were done with an applied magnetic field sweep rate of  $\sim 0.14$  T/min. Details of the calculation of the magnetic moment of the samples using this technique can be found in Appendix 1.

## 2.3 SQUID magnetometer

To check the calibration of the torque magnetometer, we performed measurements with a SQUID magnetometer MPMS XL-7 from Quantum Design, which allows measurements with an accuracy of  $\sim 10^{-8}$  emu. The sample temperature was stabilized within  $\pm 1$  mK. All measurements were done in the zero field cooled (ZFC) condition with a field sweep rate of  $\sim 0.02$  T/min.  $T_c$  was obtained from  $M(T)$  measurements of the Bi-2212 bulk crystal, performed in the ZFC regime.

## 2.4 Electrical resistivity

In order to characterize the transport properties of the Bi-2212 material, electrical resistance measurements were performed on the sample L1 (thickness of  $\simeq 22 \mu\text{m}$ , width of  $\simeq 2.2$  mm and length of  $\simeq 0.3$  mm), taken from the same bulk Bi-2212 sample. The measurements were performed as a function of temperature at fixed magnetic fields up to 2 T with the standard 4-point method. The electrodes were made with silver paste along the sample’s  $a$ - $b$  plane. Measurements were performed with an AC Resistance Bridge LR-700 from Linear Research Inc., operating with a frequency of 19 Hz and a current of  $10 \mu\text{A}$ .

### 3 Results

#### 3.1 Transport properties

The temperature dependence of the electrical resistivity of sample L1 at different applied fields, parallel to its  $c$ -axis, is shown in Figure 3 (a). The critical temperature at the middle point of the transition is  $T_c \simeq 87$  K at zero applied field. The behaviour of sample resistivity against temperature at finite fields agrees with previously reported data on the same material [34]. The high temperature resistance step clearly visible at an applied field of 2 T can be explained within a model of weakly coupled superconducting layers, where the motion of distorted vortices causes an excess dissipation [44]. Note that this phenomenon occurs at fields above 1 T and at high temperatures and it is not related to the thermally activated DL, discussed here.

The mechanism known as thermally activated flux flow (TAFF) [45] describes the thermally activated vortex motion of the FLL through a finite potential barrier  $U_0$  in the sample matrix. At low external or internal shielding currents, due to an external perturbation of the FLL, this mechanism leads to a linear (ohmic) flux flow resistivity  $\rho_{TAFF}(B, T) \simeq \rho(U_0, T) \exp(-U_0/k_B T)$ , with  $\rho(U_0, T) \propto U_0/T$ . In the first approximation, the main temperature dependence of  $\rho_{TAFF}$  follows the Arrhenius law, i.e.  $\ln(\rho)$  decreases linearly with  $T^{-1}$ , as shown in Figure 3(b). This model further predicts that a DL represents approximately a line of constant diffusivity  $D = \rho_{TAFF}/\mu_0$ , resulting in a line of constant resistivity [25, 29]. The constant resistivity line at  $\rho = 4.5 \times 10^{-5} \mu\Omega\text{cm}$  and marked in Figure 3 (b) approximately agrees with the DL, obtained from the magnetization measurements, as discussed below.

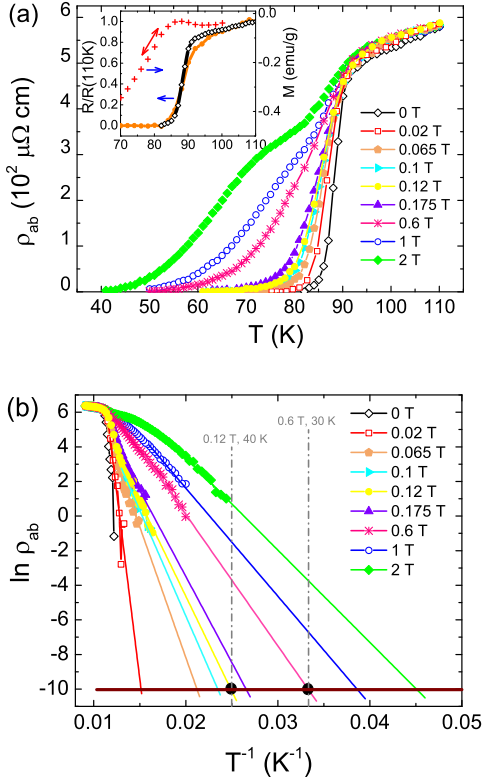


Figure 3: (a) Resistance vs. temperature of the sample L1 at different fields applied normal to the  $a$ - $b$  planes. The inset shows the temperature dependence of the resistance before ( $\bullet$ ) and after ( $\diamond$ ) the thermal treatment in air at  $120^\circ\text{C}$  for 30 min. In the inset we show also the reversible part of the magnetization temperature dependence (right  $y$ -axis). The whole measurement can be seen in Figure 10 in Appendix 3) obtained at 100 Oe applied field on the disk ( $+$ ). This disk was prepared following exactly the same procedure used to prepare the ring. The diamagnetic superconducting signal starts at the temperature where the resistance shows percolation, as expected. (b) Arrhenius plot of the same data as in (a). The thick horizontal line corresponds to a constant resistivity of  $\rho = 4.5 \times 10^{-5} \mu\Omega\text{cm}$ . The intersection points between this line and the extrapolated exponential behaviour provides a DL for a diffusion mode, compatible with that of the magnetization measurements, see Figure 6.

### 3.2 Magnetization

One magnetization field loop for the flake S1, measured in the torque magnetometer, is exemplary shown in Figure 4. To verify the accuracy of such measurements and to calibrate the absolute values of magnetic moment obtained, the flake S7, which has similar aspect ratios, was characterized in the SQUID magnetometer. The results for both samples are shown in Figure 4 and the calibration details are discussed in Appendix 1.

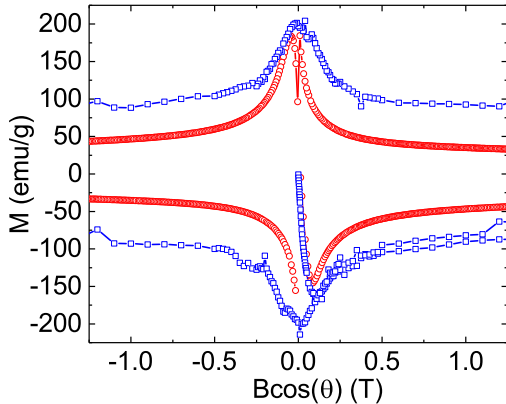


Figure 4: Magnetization hysteresis loop of the flake S1, measured with the torque magnetometer ( $\circ$ ), and the flake S7 ( $\square$ ), measured with a SQUID magnetometer. All measurements were performed at a temperature of 10 K and at an angle of  $60^\circ$  between the  $c$ -axis of the samples and the applied field.

In order to determine the DLs (or irreversibility lines) from magnetization measurements, magnetic field hysteresis loops were measured with both magnetometers at different fixed temperatures. The irreversibility field at a given temperature was determined at the field where the opening of the field loop reaches a difference between up and down field directions  $\Delta m$  of  $\pm \sim 10\%$  of the largest  $\Delta m$  measured near zero field. Magnetization hysteresis loops, obtained for the bulk sample, the flake S1 and the disk, can be seen in Figs. 8, 9 and 11 of Appendix 3. The positive applied field region of the field hysteresis for the ring sample, performed at three temperatures, is

shown in Figure 5. The depinning field was determined from the difference  $\Delta m$ , as exemplary shown in the inset of Figure 5 at 8 K. Note that the DLs of different samples were measured at different angles. Due to the significantly large anisotropy of the Bi-2212 HTSC, the DL is determined by the field component normal to the  $a$ - $b$  planes of the structure, as shown in Fig. 7 of Appendix 2.

In Figure 6 we plot the DLs obtained from these measurements for the four characterized samples, together with previously published data for bulk crystals [25]. The DLs, obtained for the bulk and flake S1 samples, agree with the DL 1 (see Figure 6). The disk DL is slightly shifted to lower relative temperatures. The DL obtained for the ring, however, shows a clear shift to significantly lower relative temperatures.

## 4 Discussion

Previous investigations [25, 26, 30, 45, 47] demonstrate that the DLs in HTSC at a given applied magnetic field (normal to the  $a$ - $b$  planes of the Bi-2212 structure) can be shifted in temperature upon the corresponding diffusion time  $\tau$  for a given sample geometry and measuring method, e.g. field sweep scans, as in our case, or AC field (susceptibility or vibrating reed) measurements. Therefore, the diffusion time in question depends on the field sweep rate (seven times shorter in the torque measurements than those by SQUID magnetometry) and sample geometry. The DL is given by a constant diffusivity  $D$  (or resistivity  $\rho_{TAF}$ ) line, defined as [25]:

$$D \simeq l_i^2 / \pi^2 \tau, \quad (1)$$

where  $l_i$  is the relevant dimension of the sample where the main diffusion mode takes place. The lower DL 1 in Figure 6 corresponds to the diffusion mode along the thickness  $t$  of the measured samples. The DLs of the flake S1 and the bulk samples are similar within experimental error. Note that any influence of the (relatively small) difference of a factor seven between the used sweep rates as well as the difference in geometry are being normalized in the selected scaling of Figure 6. This being the reason for the universal

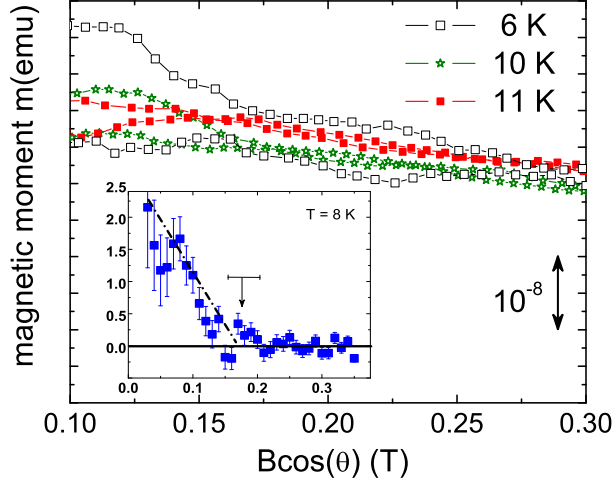


Figure 5: Magnetic moment of the Bi-2212 ring as a function of applied field at 6 K ( $\square$ ), 10 K ( $\star$ ) and 11 K ( $\blacksquare$ ). The 6 K data are presented here after subtraction of a diamagnetic line in order to show the data at the 3 temperatures in the same scale. The inset shows the difference between the up and down field sweep  $\Delta m$  measured on the Bi-2212 ring at 8 K ( $\blacksquare$ ). The irreversibility fields were determined at the values of magnetic field where  $\Delta m$  was approaching zero following [46], which are  $B_{irr} \simeq 0.295$  T at 6 K ( $\square$ ), 0.175 T at 8 K ( $\blacksquare$ ), 0.17 T at 10 K ( $\star$ ) with an error given by the horizontal bar in the middle of inset, and 0.15 T at 11 K ( $\blacksquare$ ). All measurements were obtained with the torque magnetometer at the angle  $\theta = 45^\circ$  between the  $c$ -axis of the sample and applied field.

DL obtained in a large number of Bi-2212 samples. The main result of this study, therefore, is the lack of scaling and the clear shift of the DL to lower reduced temperatures obtained for the ring sample. This result brings additional questions to our understanding of the pinning processes in HTSC.

The shifts of the DLs of the Bi-2212 ring and disk are not associated with the influence of the  $\text{Ga}^+$  irradiation during the preparation process because of

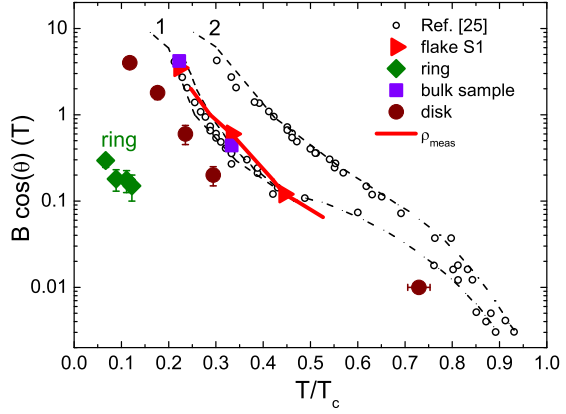


Figure 6: DLs scaling of the Bi-2212 single crystals, shown as reduced depinning temperature ( $T/T_c$ ) dependence of  $c$ -axis field component  $B_{\parallel} = B \cos \theta$ , where  $\theta$  is the angle between the  $c$ -axis of the sample and the applied field (( $\circ$ ) points are taken from [25]). DLs scaling of the bulk crystal ( $\blacksquare$ ) and the disk ( $\bullet$ ), both obtained from the magnetization hysteresis loop measurements in a SQUID magnetometer at the angle  $\theta = 0^\circ$ ; the flake S1, measured in a torque magnetometer at the angle  $\theta = 60^\circ$  ( $\blacktriangleright$ ); and the ring, measured in a torque magnetometer at the angle  $\theta = 45^\circ$  ( $\blacklozenge$ ). The solid line corresponds to the constant resistivity  $\rho_{ab}$  line, obtained from resistance measurement of Bi-2212 sample L1, shown in Figure 3.

the following reasons: (i) the samples were protected before preparation with a 1  $\mu\text{m}$  thick layer of PMMA, which prevents the entering of the  $\text{Ga}^+$  ions into the main part of the samples. (ii) In the case that some Ga doping would occur, the DL shift to higher reduced temperatures might be expected with the increase in the number of defects [38, 48–54]. Also, the electrical resistivity measurements, as well as the magnetization measurement (inset in Figure 3(a), Figure 10), revealed that the annealing treatment in air nor the FIB using  $\text{Ga}^+$  ions do not decrease the  $T_c$  of the sample. Furthermore, there is no decrease of  $T_c$  with the reduction of the sample thickness of Bi-2212 HTSC [8].

What about the influence of the geometrical bar-



rier? A shift to lower temperatures of the DL has been observed at  $T \geq 76$  K in Ref. [31] when the Bi-2212 sample was polished from a platelet geometry into a prism shape, i.e. thereby reducing the geometrical barrier. We note, however, that the main pinning potential, that influences the DLs shown in Figure 6, is not related to the influence of the geometrical barrier, at least in the low reduced temperature region. Moreover, we do not expect any change in the influence of the geometrical barrier because the edge shape of the flakes or bulk samples and of the ring are similar.

It was experimentally shown that the irreversibility field can decrease in Bi-2212 single crystals and films when the thickness of the samples is less than the pinning correlation length  $L_0$ , which for Bi-2212 is estimated to be  $\sim 10 \mu\text{m}$  [55]. This phenomenon is also manifested in the DL of the disk, obtained from the magnetic measurements. In this case, we expect a reduction of the pinning potential  $U_0$  if the thickness of the sample decreases. According to Refs. [55–57], a decrease of a factor of two in the thickness  $t < L_0$  between the ring and flake S1 may produce a similar decrease in  $U_0$ . Moreover, the decrease of the sample thickness can produce an extra decrease in the pinning potential of the FLL if the thickness is of the order or smaller than the London penetration depth  $\lambda$  ( $\sim 4 \mu\text{m}$  at low temperatures). Under such circumstance, the penetration depth is replaced by the Pearl’s effective length  $\Lambda = 2\lambda^2/t \gg \lambda$  [58]. A broadening of the effective size of a vortex is expected to decrease the pinning potential and, therefore, the DL. These so-called Pearl vortices have been recently visualized in narrow flat rings, made of amorphous MoGe superconducting thin films [59], as well as in Y-123 HTSC thin films [60].

Therefore, the DL shift in the thin Bi-2212 ring can be interpreted as a result of the double size effect: a decrease in the pinning potential when the thickness is below the correlation length  $L_0$  and the increase in the external size of the vortices (Pearl’s vortices). This shift of the DL can have a detrimental effect on the possible applications of thin rings as antennas or emitters. A possible solution to reduce this influence could be a strong doping of the device, although the shift of the DL through doping remains

rather restricted [38, 48–54].

## 5 Conclusions

In summary, we demonstrated that the DL of Bi-2212 can be significantly shifted to lower reduced temperatures. This large detrimental effect on the DL is attributed to the double size effect, where the small thickness of the narrow ring plays a main role. This effect should be taken into account when considering HTSC-based devices for THz range application as proposed in Ref. [2].

## Acknowledgements

We thank A. Deutschinger, F. Bern and C. E. Precker for the technical assistance and M. Lorenz for helpful discussions. B. S. acknowledges the partial financial support from Erasmus Mundus Webb project no. 2012-27.39/001-001-EM and the partial financial support from DAAD-Programm STIBET; B. C. C. acknowledges the financial support from the National Science Center, Poland, research project no. 2016/23/P/ST3/03514 within the POLONEZ programme. The POLONEZ programme has received funding from the European Union’s Horizon 2020 research and innovation programme under the Marie SkłodowskaCurie grant agreement No. 665778. Y. K. was supported by FAPESP and CNPq.

## Appendix 1: Details of torque magnetometry and the calibration of the device

To calculate the magnetic moment of the sample from the measured resistance in the Wheatstone bridge, the following equation was used:

$$m = \frac{k\Delta x l}{B \sin(\theta)}, \quad (2)$$

where  $m$  is the magnetic moment of the sample,  $\Delta x$  is the measured deflection at the edge of the cantilever tip,  $\theta$  is the angle between the magnetic moment and

magnetic field  $B$ ,  $l$  is the length of the cantilever tip. Since the cantilevers have piezoresistors as a deflection sensor, their sensitivity is described by the following equation [61–64]:

$$\frac{\Delta R}{R_0} = GF \frac{\Delta x}{l}, \quad (3)$$

where  $\Delta R$  is a resistance change of the piezoresistor,  $R_0$  is a resistance of a piezoresistance in undeflected state,  $GF$  is a gauge factor.

In order to estimate the deflection at the edge of the cantilever tip  $\Delta x$ , the calibration of the cantilevers were performed. The gauge factor  $GF$  of the cantilever, that was used for the Bi-2212 ring, was mechanically determined by a manipulator from SURUGA SEIKI CO., LTD, using the method described elsewhere [43, 63]. Further calibration of the  $GF$  was performed in the SQUID magnetometer by measuring the magnetization of the Bi-2212 flake S7, that has the identical geometry ratio [65] as the Bi-2212 sample S1, see Figure 4. Calibration was performed along the part of hysteresis line from the zero field to the critical field  $B_{c1}$ , since this is the part of the loop where pinning processes do not manifest.

To determine the spring constant  $k$ , the equation was used from Ref. [66]:

$$k = \frac{Et_c^3 w}{4l^3}, \quad (4)$$

where  $w$  is the width,  $l$  is the length of the cantilever tip,  $t_c$  is the cantilever thickness and  $E = 1.7 \cdot 10^{11}$  Pa is the Young modulus.

The parameters of the cantilevers, used in our experiments, are presented in Table 2.

We took into account that at low temperatures the geometric parameters of cantilevers do not change significantly, the Young modulus increases by  $\sim 2\%$  [67, 68], and the piezoresistive coefficients increase by  $\sim 20\%$  [63], and  $R_0$  decreases by  $\sim 20\%$ . The temperature sensitivity of the cantilevers was also taken into account to calculate the magnetic moment of the samples.

Table 2: Parameters of the cantilevers used for the measurements with the torque magnetometer: the length ( $l$ ), the width ( $w$ ), the thickness ( $t_c$ ) and the spring constant of the cantilever tip ( $k$ ), the resistance of the piezoresistor in undeflected state ( $R_0$ ) and the gauge factor ( $GF$ ).

Cantilever No.	$l$ [ $\mu\text{m}$ ]	$w$ [ $\mu\text{m}$ ]	$t_c$ [ $\mu\text{m}$ ]	$k$ [N/m]	$R_0$ [k $\Omega$ ]	$GF$	sample
198	305	110	3.8	9.0	1.196	0.78	ring
211	305	110	4.0	10.5	1.165	0.69	flake S1

## Appendix 2: Magnetization of the Bi-2212 flake S7 at two angles

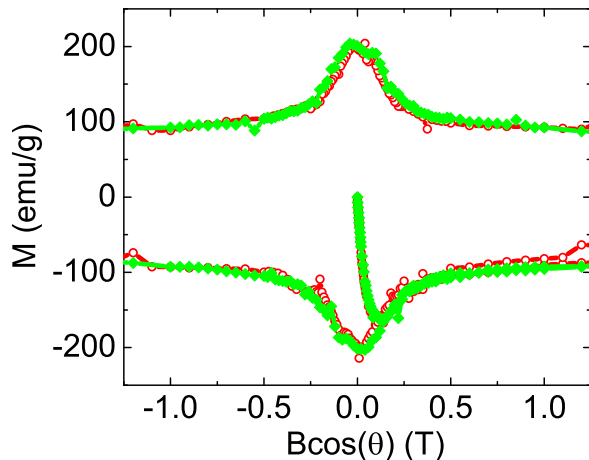


Figure 7: Field dependence of the magnetization of the Bi-2212 flake S7, measured with the SQUID magnetometer at the temperature of 10 K and at angles  $0^\circ$  ( $\blacklozenge$ ) and  $60^\circ$  ( $\circ$ ) between the  $c$ -axis of the sample and the applied field.

Measurements of the hysteresis loops at 2 angles were carried out for the Bi-2212 flake S7 using the



SQUID magnetometer (Figure 7). These measurements indicate that the angle between the  $c$ -axis of sample and the field does not affect the pinning mechanism in Bi-2212 flakes.

### Appendix 3: Magnetization of the Bi-2212 bulk crystal, flake S1 and disk

The magnetization hysteresis loops for the flake S7 (Figure 7), the bulk crystal (Figure 8) and the disk (Figure 11), measured by the SQUID magnetometer, and the magnetization hysteresis loops of the Bi-2212 flake S1 (Figs. 4 and 9), measured by the torque magnetometer, show a typical superconducting behaviour and are comparable with the results, reported in Ref. [69–78].

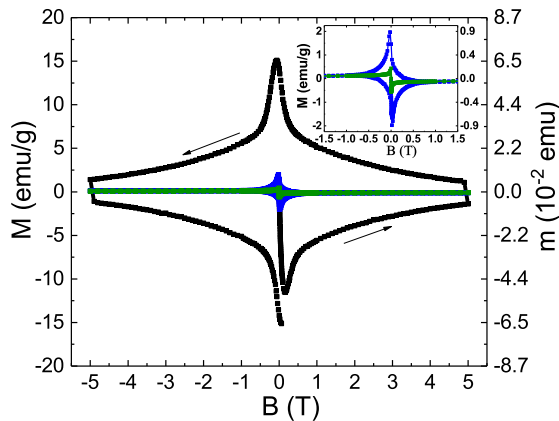


Figure 8: Magnetization of the Bi-2212 bulk crystal versus the applied field at  $T = 10$  K (■), 20 K (●) and 30 K (▲), obtained with the SQUID magnetometer. The  $c$ -axis of the sample was parallel to the applied field.

The ZFC and FC magnetization measurements of the disk at 100 Oe (Figure 10) shows also a typical superconducting behaviour. As can be seen from Figure 10,  $T_c$  of the superconducting disk is observed at  $\sim 85$  K, which indicates the absence of a significant effect of annealing at  $120^\circ\text{C}$  and irradiation by

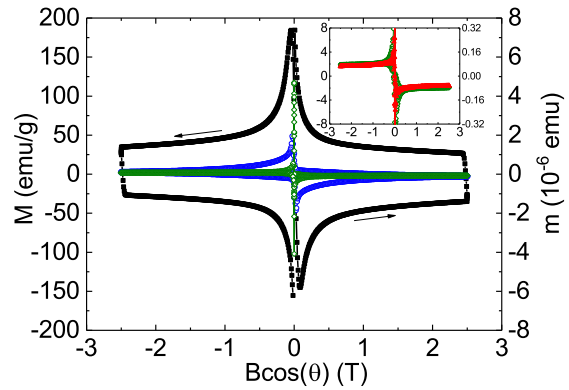


Figure 9: Magnetization of the Bi-2212 flake S1 versus the applied field at 10 K (■), 20 K (○), 30 K (◇) and 40 K (▲), obtained with the torque magnetometer at the angle  $\theta = 60^\circ$  between the  $c$ -axis of the sample and the applied field.

gallium ions on the  $T_c$  of the samples.

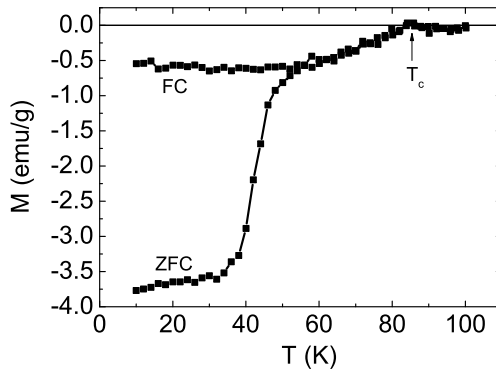


Figure 10: Magnetization of the Bi-2212 disk as a function of temperature at fixed magnetic field 100 Oe.

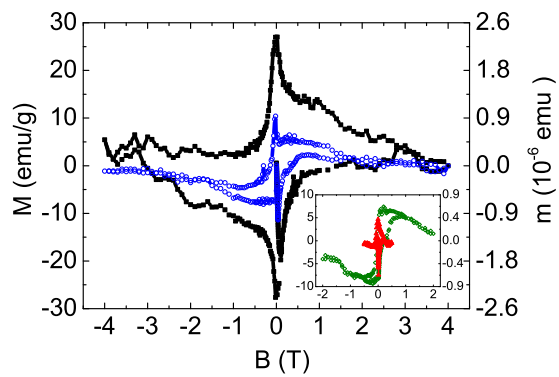


Figure 11: Magnetization of the Bi-2212 disk versus the applied field at 10 K (■), 15 K (○), 20 K (◇) and 25 K (▲), obtained with the SQUID magnetometer at the angle  $\theta = 0^\circ$  between the  $c$ -axis of the sample and the applied field.

## References

- [1] Y. Huang, H. Miao, S. Hong, J.A. Parrell, IEEE Transactions on Applied Superconductivity **24**(3), 1 (2014). DOI 10.1109/TASC.2013.2281063
- [2] S. Kalhor, M. Ghanaatshoar, T. Kashiwagi, K. Kadowaki, M.J. Kelly, K. Delfanazari, IEEE Photonics Journal **9**(5), 1 (2017). DOI 10.1109/JPHOT.2017.2754465
- [3] O.V. Kharissova, E.M. Kopnin, V.V. Maltsev, N.I. Leonyuk, L.M. León-Rossano, I.Y. Pinus, B.I. Kharisov, Critical Reviews in Solid State and Materials Sciences **39**(4), 253 (2014). DOI 10.1080/10408436.2013.836073
- [4] Y. Saito, T. Nojima, Y. Iwasa, Nature Reviews Materials **2**(16094) (2016). DOI 10.1038/natrevmats.2016.94
- [5] K. Sato, in *Superconductors in the Power Grid*, ed. by C. Rey, Woodhead Publishing Series in Energy (Woodhead Publishing, 2015), pp. 75 – 95. DOI <https://doi.org/10.1016/B978-1-78242-029-3.00003-0>
- [6] T. Semerci, Y. Demirhan, N. Miyakawa, H.B. Wang, L. Ozyuzer, Optical and Quantum Electronics **48**(6), 340 (2016). DOI 10.1007/s11082-016-0612-0
- [7] M. Liao, Y. Zhu, J. Zhang, R. Zhong, J. Schneeloch, G. Gu, K. Jiang, D. Zhang, X. Ma, Q.K. Xue, Nano letters **18**(9), 5660 (2018). DOI [doi:10.1021/acs.nanolett.8b02183](https://doi.org/10.1021/acs.nanolett.8b02183)
- [8] Y. Yu, L. Ma, P. Cai, R. Zhong, C. Ye, J. Shen, G. Gu, X.H. Chen, Y. Zhang, Nature pp. 156–163 (2019). DOI <https://doi.org/10.1038/s41586-019-1718-x>
- [9] H. Minami, Y. Ono, K. Murayama, Y. Tanabe, K. Nakamura, S. Kusunose, T. Kashiwagi, M. Tsujimoto, K. Kadowaki, Journal of Physics: Conference Series **1293**, 012056 (2019). DOI 10.1088/1742-6596/1293/1/012056
- [10] T.M. Benseman, A.E. Koshelev, V. Vlasko-Vlasov, Y. Hao, U. Welp, W.K. Kwok, B. Gross, M. Lange, D. Koelle, R. Kleiner, H. Minami, M. Tsujimoto, K. Kadowaki, Phys. Rev. B **100**, 144503 (2019). DOI 10.1103/PhysRevB.100.144503
- [11] K. Delfanazari, R.A. Klemm, M. Tsujimoto, D.P. Cerkoney, T. Yamamoto, T. Kashiwagi, K. Kadowaki, Journal of Physics: Conference Series **1182**, 012011 (2019). DOI 10.1088/1742-6596/1182/1/012011
- [12] R. Kleiner, H. Wang, Journal of Applied Physics **126**(17), 171101 (2019). DOI 10.1063/1.5116660
- [13] E.H. Brandt, Phys. Rev. B **55**, 14513 (1997). DOI 10.1103/PhysRevB.55.14513
- [14] E.H. Brandt, Phys. Rev. B **58**, 6506 (1998). DOI 10.1103/PhysRevB.58.6506
- [15] E.H. Brandt, Phys. Rev. B **58**, 6523 (1998). DOI 10.1103/PhysRevB.58.6523
- [16] C. Navau, A. Sanchez, E. Pardo, D.X. Chen, E. Bartolomé, X. Granados, T. Puig, X. Obradors, Phys. Rev. B **71**, 214507 (2005). DOI 10.1103/PhysRevB.71.214507
- [17] A. Sanchez, C. Navau, Phys. Rev. B **64**, 214506 (2001). DOI 10.1103/PhysRevB.64.214506
- [18] C. Gough, A. Gencer, G. Yang, M. Shoustari, A. Rae, J. Abell, Cryogenics **33**(3), 339 (1993). DOI [https://doi.org/10.1016/0011-2275\(93\)90056-T](https://doi.org/10.1016/0011-2275(93)90056-T). Critical Currents in High  $T_c$  Superconductors
- [19] F. Mrowka, M. Wopturlitzer, P. Esquinazi, E.H. Brandt, M. Lorenz, K. Zimmer, Applied Physics Letters **70**(7), 898 (1997). DOI 10.1063/1.118308
- [20] M. Pannetier, F.C. Klaassen, R.J. Wijngaarden, M. Welling, K. Heeck, J.M. Huijbregtse, B. Dam, R. Griessen, Phys. Rev. B **64**, 144505 (2001). DOI 10.1103/PhysRevB.64.144505

- [21] K. Schindler, M. Ziese, P. Esquinazi, H. Hochmuth, M. Lorenz, K. Zimmer, E. Brandt, *Physica C: Superconductivity* **417**(3), 141 (2005). DOI <https://doi.org/10.1016/j.physc.2004.10.013>
- [22] S. Streubel, F. Mrowka, M. Wopturlitzer, P. Esquinazi, K. Zimmer, *Journal of Applied Physics* **87**(12), 8621 (2000). DOI 10.1063/1.373531
- [23] Y.Y. Xue, Z.J. Huang, P.H. Hor, C.W. Chu, *Phys. Rev. B* **43**, 13598 (1991). DOI 10.1103/PhysRevB.43.13598
- [24] H. Bluhm, N.C. Koshnick, M.E. Huber, K.A. Moler, *Phys. Rev. Lett.* **97**, 237002 (2006). DOI 10.1103/PhysRevLett.97.237002
- [25] M. Ziese, P. Esquinazi, H.F. Braun, *Superconductor Science and Technology* **7**(12), 869 (1994)
- [26] Y. Kopelevich, A. Gupta, P. Esquinazi, *Phys. Rev. Lett.* **70**, 666 (1993). DOI 10.1103/PhysRevLett.70.666
- [27] A. Gupta, P. Esquinazi, H.F. Braun, W. Gerhäuser, H.W. Neumüller, K. Heine, J. Tenbrink, *EPL (Europhysics Letters)* **10**(7), 663 (1989)
- [28] A. Gupta, P. Esquinazi, H.F. Braun, H.W. Neumüller, *Phys. Rev. Lett.* **63**, 1869 (1989). DOI 10.1103/PhysRevLett.63.1869
- [29] P. Esquinazi, *J Low Temp Phys* **85**(3-4), 139 (1991). DOI <https://doi.org/10.1007/BF00681969>
- [30] A. Gupta, Y. Kopelevich, M. Ziese, P. Esquinazi, P. Fischer, F.I. Schulz, H.F. Braun, *Phys. Rev. B* **48**, 6359 (1993). DOI 10.1103/PhysRevB.48.6359
- [31] D. Majer, E. Zeldov, M. Konczykowski, *Phys. Rev. Lett.* **75**, 1166 (1995). DOI 10.1103/PhysRevLett.75.1166
- [32] B. Kalisky, A. Shaulov, Y. Yeshurun, *Pramana* **66**(1), 141 (2006). DOI 10.1007/BF02704943
- [33] Y. Kopelevich, S. Moehlecke, J.H.S. Torres, R.R. da Silva, P. Esquinazi, *Journal of Low Temperature Physics* **116**(3), 261 (1999). DOI 10.1023/A:1021893818924
- [34] J. Torres, R.R. da Silva, S. Moehlecke, Y. Kopelevich, *Solid State Communications* **125**(1), 11 (2003). DOI [https://doi.org/10.1016/S0038-1098\(02\)00629-4](https://doi.org/10.1016/S0038-1098(02)00629-4)
- [35] H. Fujishiro, M. Ikebe, T. Naito, M. Matsukawa, K. Noto, I. Shigaki, K. Shibusaki, S. Hayashi, R. Ogawa, *Physica C: Superconductivity* **235-240**, 1533 (1994). DOI [https://doi.org/10.1016/0921-4534\(94\)91991-7](https://doi.org/10.1016/0921-4534(94)91991-7)
- [36] D.E. Farrell, S. Bonham, J. Foster, Y.C. Chang, P.Z. Jiang, K.G. Vandervoort, D.J. Lam, V.G. Kogan, *Phys. Rev. Lett.* **63**, 782 (1989). DOI 10.1103/PhysRevLett.63.782
- [37] G.D. Gu, R. Puzniak, K. Nakao, G.J. Russell, N. Koshizuka, *Superconductor Science and Technology* **11**(10), 1115 (1998)
- [38] T. Haraguchi, S. Takayama, M. Kiuchi, E. Otabe, T. Matsushita, T. Yasuda, S. Okayasu, S. Uchida, J. Shimoyama, K. Kishio, *Physica C: Superconductivity and its Applications* **445-448**, 123 (2006). DOI <https://doi.org/10.1016/j.physc.2006.03.092>. Proceedings of the 18th International Symposium on Superconductivity (ISS 2005)
- [39] N. Musolino, S. Bals, G. van Tendeloo, N. Clayton, E. Walker, R. Flükiger, *Physica C: Superconductivity* **399**(1), 1 (2003). DOI [https://doi.org/10.1016/S0921-4534\(03\)01324-8](https://doi.org/10.1016/S0921-4534(03)01324-8)
- [40] J. Ricketts, R. Puzniak, C. Liu, G.D. Gu, N. Koshizuka, H. Yamauchi, *Applied Physics Letters* **65**(25), 3284 (1994). DOI 10.1063/1.112438
- [41] F. Steinmeyer, R. Kleiner, P. Müller, H. Müller, K. Winzer, *EPL (Europhysics Letters)* **25**(6), 459 (1994)

- [42] Keysight Technologies, *Application Note: Imaging with Self-Sensing Cantilever on Keysight 5500/5600LS Atomic Force Microscopes*. URL <http://literature.cdn.keysight.com/litweb/pdf/5999-2481EN.pdf> (2018).
- [43] B. Semenenko, P.D. Esquinazi, *Magnetochemistry* **4**(4) (2018). DOI 10.3390/magnetochemistry4040052
- [44] J.W.P. Hsu, D.B. Mitzi, A. Kapitulnik, M. Lee, *Phys. Rev. Lett.* **67**, 2095 (1991). DOI 10.1103/PhysRevLett.67.2095
- [45] P.H. Kes, J. Aarts, J. van den Berg, C.J. van der Beek, J.A. Mydosh, *Superconductor Science and Technology* **1**(5), 242 (1989). DOI 10.1088/0953-2048/1/5/005
- [46] F. Supple, A. Campbell, J. Cooper, *Physica C: Superconductivity* **242**(3), 233 (1995). DOI [https://doi.org/10.1016/0921-4534\(94\)02411-1](https://doi.org/10.1016/0921-4534(94)02411-1)
- [47] E.H. Brandt, *Phys. Rev. Lett.* **68**, 3769 (1992). DOI 10.1103/PhysRevLett.68.3769
- [48] H. Kumakura, H. Kitaguchi, K. Togano, H. Maeda, J. Shimoyama, S. Okayasu, Y. Kazumata, *Journal of Applied Physics* **74**(1), 451 (1993). DOI 10.1063/1.355279
- [49] A.K. Pradhan, S.B. Roy, P. Chaddah, D. Kanjilal, C. Chen, B.M. Wanklyn, *Phys. Rev. B* **53**, 2269 (1996). DOI 10.1103/PhysRevB.53.2269
- [50] G. Villard, D. Pelloquin, A. Maignan, A. Wahl, *Applied Physics Letters* **69**(10), 1480 (1996). DOI 10.1063/1.116914
- [51] T.W. Li, R.J. Drost, P.H. Kes, C. Træholt, H.W. Zandbergen, N.T. Hien, A.A. Menovsky, J.J.M. Franse, *Physica C: Superconductivity* **274**(3), 197 (1997). DOI [https://doi.org/10.1016/S0921-4534\(96\)00699-5](https://doi.org/10.1016/S0921-4534(96)00699-5)
- [52] Y.P. Sun, W.H. Song, B. Zhao, J.J. Du, H.H. Wen, Z.X. Zhao, H.C. Ku, *Applied Physics Letters* **76**(25), 3795 (2000). DOI 10.1063/1.126784
- [53] T. Haraguchi, T. Imada, M. Kiuchi, E. Otabe, T. Matsushita, T. Yasuda, S. Okayasu, S. Uchida, J. Shimoyama, K. Kishio, *Physica C: Superconductivity* **426-432**, 364 (2005). DOI <https://doi.org/10.1016/j.physc.2005.01.026>. Proceedings of the 17th International Symposium on Superconductivity (ISS 2004)
- [54] N. Panarina, D. Bizyaev, V. Petukhov, Y. Talanov, *Physica C: Superconductivity* **470**(4), 251 (2010). DOI <https://doi.org/10.1016/j.physc.2009.09.008>
- [55] T. Matsushita, M. Kiuchi, T. Yasuda, H. Wada, T. Uchiyama, I. Iguchi, *Superconductor Science and Technology* **18**(10), 1348 (2005)
- [56] N. Ihara, T. Matsushita, *Physica C: Superconductivity and its Applications* **257**(3), 223 (1996). DOI [https://doi.org/10.1016/0921-4534\(95\)00534-X](https://doi.org/10.1016/0921-4534(95)00534-X)
- [57] T. Matsushita, E.S. Otabe, H. Wada, Y. Takahama, H. Yamauchi, *Physica C: Superconductivity* **397**(1), 38 (2003). DOI [https://doi.org/10.1016/S0921-4534\(03\)01085-2](https://doi.org/10.1016/S0921-4534(03)01085-2)
- [58] J. Pearl, *Applied Physics Letters* **5**(4), 65 (1964). DOI 10.1063/1.1754056
- [59] N. Kokubo, S. Okayasu, T. Nojima, *Journal of Applied Physics* **125**(22), 223906 (2019). DOI 10.1063/1.5100497
- [60] V.M. Acosta, L.S. Bouchard, D. Budker, R. Folman, T. Lenz, P. Maletinsky, D. Rohner, Y. Schlüssel, L. Thiel, *J Supercond Nov Magn* **32**, 85 (2019). DOI <https://doi.org/10.1007/s10948-018-4877-3>
- [61] A.A. Barlian, W.T. Park, J.R. Mallon, A.J. Rastegar, B.L. Pruitt, *Proceedings of the IEEE* **97**(3), 513 (2009). DOI 10.1109/JPROC.2009.2013612
- [62] Y. Kanda, *Sensors and Actuators A: Physical* **28**(2), 83 (1991). DOI [https://doi.org/10.1016/0924-4247\(91\)85017-I](https://doi.org/10.1016/0924-4247(91)85017-I)

- [63] J.Y.W. Seto, *Journal of Applied Physics* **47**(11), 4780 (1976). DOI 10.1063/1.322515
- [64] X. Yu, J. Thaysen, O. Hansen, A. Boisen, *Journal of Applied Physics* **92**(10), 6296 (2002). DOI 10.1063/1.1493660
- [65] Y.M. Wang, M.S. Fuhrer, A. Zettl, S. Ooi, T. Tamegai, *Phys. Rev. Lett.* **86**, 3626 (2001). DOI 10.1103/PhysRevLett.86.3626
- [66] M.A. Poggi, A.W. McFarland, J.S. Colton, L.A. Bottomley, *Analytical Chemistry* **77**(4), 1192 (2005). DOI 10.1021/ac048828h. PMID: 15859006
- [67] J.C. Greenwood, *Journal of Physics E: Scientific Instruments* **21**(12), 1114 (1988). URL <http://stacks.iop.org/0022-3735/21/i=12/a=961>
- [68] J. hyun Jeong, S. hoon Chung, S.H. Lee, D. Kwon, *Journal of Microelectromechanical Systems* **12**(4), 524 (2003). DOI 10.1109/JMEMS.2003.811733
- [69] S.X. Dou, X.L. Wang, Y.C. Guo, Q.Y. Hu, P. Mikheenko, J. Horvat, M. Ionescu, H.K. Liu, *Superconductor Science and Technology* **10**(7A), A52 (1997)
- [70] H. Fallah-Arani, S. Baghshahi, A. Sedghi, D. Stornaiuolo, F. Tafuri, N. Riahi-Noori, *Physica C: Superconductivity and its Applications* **548**, 31 (2018). DOI <https://doi.org/10.1016/j.physc.2018.01.012>
- [71] K. Fossheim, E.D. Tuset, T.W. Ebbesen, M.M.J. Treacy, J. Schwartz, *Physica C: Superconductivity* **248**(3), 195 (1995). DOI [https://doi.org/10.1016/0921-4534\(95\)00382-7](https://doi.org/10.1016/0921-4534(95)00382-7)
- [72] S. ichiro Hatta, K. Hirochi, H. Adachi, T. Kamada, Y. Ichikawa, K. Setsune, K. Wasa, *Japanese Journal of Applied Physics* **27**(9R), 1646 (1988)
- [73] K. Kishio, S. Komiya, N. Motohira, K. Kitazawa, K. Yamafuji, *Physica C: Superconductivity* **185-189**, 2377 (1991). DOI [https://doi.org/10.1016/0921-4534\(91\)91313-S](https://doi.org/10.1016/0921-4534(91)91313-S)
- [74] W. Kritscha, F. Sauerzopf, H. Weber, G. Crabtree, Y. Chang, P. Jiang, *Physica C: Superconductivity* **179**(1), 59 (1991). DOI [https://doi.org/10.1016/0921-4534\(91\)90011-M](https://doi.org/10.1016/0921-4534(91)90011-M)
- [75] R. Noetzel, B. vom Hedt, K. Westerholt, *Physica C: Superconductivity* **260**(3), 290 (1996). DOI [https://doi.org/10.1016/0921-4534\(96\)00146-3](https://doi.org/10.1016/0921-4534(96)00146-3)
- [76] G. Ries, H.W. Neumuller, W. Schmidt, *Superconductor Science and Technology* **5**(1S), S81 (1992)
- [77] B. Özçelik, O. Nane, A. Sotelo, M. Madre, *Ceramics International* **42**(2, Part B), 3418 (2016). DOI <https://doi.org/10.1016/j.ceramint.2015.10.137>
- [78] H. Öztürk, S. Safran, *Journal of Alloys and Compounds* **731**, 831 (2018). DOI <https://doi.org/10.1016/j.jallcom.2017.10.095>